A comparison of united atom, explicit atom, and coarse-grained simulation models for poly(ethylene oxide)

Chunxia Chen and Praveen Depa
Department of Chemical Engineering, The Pennsylvania State University, University Park, Pennsylvania 16802

Victoria García Sakai
Department of Materials Science and Engineering, University of Maryland, College Park, Maryland 20742

Janna K. Maranas[a]
Department of Chemical Engineering, The Pennsylvania State University, University Park, Pennsylvania 16802

Jeffrey W. Lynn
NIST Center for Neutron Research, National Institute of Standards and Technology, Gaithersburg, Maryland 20899

Inmaculada Peral[b]
Department of Materials Science and Engineering, University of Maryland, College Park, Maryland 20742

John R. D. Copley
NIST Center for Neutron Research, National Institute of Standards and Technology, Gaithersburg, Maryland 20899

We compare static and dynamic properties obtained from three levels of modeling for molecular dynamics simulation of poly(ethylene oxide) (PEO). Neutron scattering data are used as a test of each model's accuracy. The three simulation models are an explicit atom (EA) model (all the hydrogens are taken into account explicitly), a united atom (UA) model (CH_2 and CH_3 groups are considered as a single unit), and a coarse-grained (CG) model (six united atoms are taken as one bead). All three models accurately describe the PEO static structure factor as measured by neutron diffraction. Dynamics are assessed by comparison to neutron time of flight data, which follow self-motion of protons. Hydrogen atom motion from the EA model and carbon/oxygen atom motion from the UA model closely follow the experimental hydrogen motion, while hydrogen atoms reinserted in the UA model are too fast. The EA and UA models provide a good description of the orientation properties of C–H vectors measured by nuclear magnetic resonance experiments. Although dynamic observables in the CG model are in excellent agreement with their united atom counterparts, they cannot be compared to neutron data because the time after which the CG model is valid is greater than the neutron decay times. © *2006 American Institute of Physics.* [DOI: 10.1063/1.2204035]

I. INTRODUCTION

Dynamics in polymers span a broad range of temporal and spatial scales. As a result, a full understanding of polymer dynamics requires connecting models at several length and time scales (often referred to as "multiscale modeling").[1,2] Molecular dynamics (MD), which describes the movement of all the particles of a molecular system by iteratively solving Newton's equations of motion, has been used widely for understanding the chemical and physical properties of various materials on various length and time scales. Several levels of detail are possible while still main-taining the chemical identity of the chain. The first, an explicit atom (EA) model, treats all atoms including hydrogen as interaction sites. The second, a united atom (UA) model, reduces computation time by grouping each carbon with its bonded hydrogen atoms to form a united atom. The third, a coarse-grained (CG) model, reduces computation time even further by grouping a few united atoms, monomers, or even the whole chain as a single CG bead. There are some instances where EA modeling is required, for example, in the calculation of properties such as the vibrational density of states, methyl group rotation, and elastic constants of crystalline polymers. The UA representation is widely used because it is computationally efficient while providing results in reasonable agreement with available experimental data. For the same reason, CG models are becoming more common.

---

[a]Electronic mail: jmaranas@psu.edu
[b]Present address: Institut de Ciencia de Materials de Barcelona (CSIC), Campus de la Universitat Autonoma de Barcelona, 08193, Bellaterra, Barcelona, Spain.

124, 234901-1

TABLE I. UA model parameters.

Bonds	$u^{\text{bond}}(r_{ij}) = \dfrac{k_{\text{bond}}}{2}(r_{ij} - r_{ij}^0)^2$	
	k_{bond} (kJ/mol Å^2)	r_{ij}^0 (Å)
C–C	2587.4	1.54
C–O	3094.0	1.43

Bends	$u^{\text{bend}}(\theta_{jjk}) = \dfrac{k_{\text{bend}}}{2}(\cos\theta_{jjk} - \cos\theta_{ijk}^0)^2$	
	k_{bend} (kJ/mol)	θ_{ijk}^0 (deg)
O–C–C	727.7	110.0
C–O–C	1070.1	112.0

Torsion (kJ/mol)	$u^{\text{torsion}}(\phi_{ijkl}) = \Sigma_{k=0}^{6} a_k \cos^k \phi_{ijkl}$						
	a_0	a_1	a_2	a_3	a_4	a_5	a_6
O–C–C–O	2.211	15.194	17.844	−32.460	−13.871	−1.189	12.322
C–C–O–C	5.183	5.610	6.272	−15.428	−0.678	−4.568	3.567

Nonbonded interaction	$u^{\text{nb}}(r_{ij}) = \varepsilon_{ij}\left[\left(\dfrac{\sigma_{ij}}{r_{ij}}\right)^{12} - 2\left(\dfrac{\sigma_{ij}}{r_{ij}}\right)^{6}\right] + \dfrac{1}{4\pi\varepsilon_0}\dfrac{q_i q_j}{r_{ij}}$	
Mixing rules	$\sigma_{ij} = \dfrac{1}{2}\sigma_i + \dfrac{1}{2}\sigma_j$	$\varepsilon_{ij} = \sqrt{\varepsilon_i \varepsilon_j}$
	σ_i (Å) ε_i (kJ/mol)	q_i (e.c.)
CH$_3$	4.152 1.047	0
CH$_2$	4.068 0.831	0.174
O	3.405 0.401	−0.348

Force fields for EA and UA models are highly developed for many materials. They are typically obtained from *ab initio* calculations or by tuning parameters to experimental observables. A series of comparison studies[3–6] has been conducted on *n*-alkanes using EA and UA models. It was shown that both EA and UA models quantitatively reproduced both structural and dynamic data. McCoy and co-workers[7,8] proposed a UA/EA mapping procedure to obtain a UA potential from an EA potential which was tested on C$_{20}$H$_{42}$ and C$_{48}$H$_{98}$ in the liquid state. They found excellent agreement between liquid structure and chain dimensions from the two models, but the UA potential obtained from UA/EA mapping exhibited attractions that were too strong, as evidenced by a negative pressure and high compressibility.

Some CG models made no attempt to differentiate between chemical structures, but recently CG models have appeared that are linked directly to an underlying chemically detailed model.[9–11] Two methods have been used to provide this link. In one approach, the static properties are matched and correct dynamic evolution is ensured by adjusting the friction frequency appearing in Langevin's equations of motion. Langevin dynamics are then used to evolve the system in time.[12–14] In the other method, the bonded and nonbonded potentials for CG models are derived from mapping the distribution functions with those from atomistic simulations, but no measure is taken to enforce correct dynamic evolution. This method successfully reproduces structural properties,

but dynamic properties obtained using it are typically faster than those from atomistic simulations.[15–17] For polyethylene (PE) the origin of this "indirect speedup" is a reduced attraction to neighboring chains caused by the change in Lennard-Jones (LJ) potentials required to match intermolecular structure to the underlying UA model.[18] To obtain correct dynamic evolution, the time step is scaled by a constant, after which CG dynamic observables are in excellent agreement with their united atom counterparts.

Our objective is to determine the effect of coarse graining on static and dynamic properties by comparing results from the EA, UA, and CG levels of description. We take existing EA and UA force fields (described below) and provide our own CG force field using procedures described earlier. Poly(ethylene oxide) (PEO) has attracted a lot of attention because of its wide applications ranging from use as a solid polymer electrolyte to treatment of surfaces for resistance to protein adsorption. EA models for PEO have been developed by Smith and co-workers[19–22] and Neyertz *et al.*[23] The model of Smith and co-workers agrees with experimental data for both static and dynamic properties, while the model of Neyertz *et al.* reproduces the structures of crystalline and melt PEO. van Zon *et al.*[24] obtained a UA force field based on a modification of the EA force field of Neyertz *et al.* and showed that the intermediate scattering function calculated from this UA model is in good agreement with neu-

TABLE II. EA model parameters.

Bonds	$u^{bond}(r_{ij}) = \dfrac{k_{bond}}{2}(r_{ij} - r_{ij}^0)^2$	
	k_{bond} (kJ/mol Å^2)	r_{ij}^0 (Å)
C–C	2587.4	1.513
C–O	3094.0	1.390
C–H	2742.4	1.090

Bends	$u^{bend}(\theta_{ijk}) = \dfrac{k_{bend}}{2}(\theta_{ijk} - \theta_{ijk}^0)^2$	
	k_{bend} (kJ/mol rad)	θ_{ijk}^0 (deg)
C–C–H	359.2	458.4
H–C–H	322.6	453.4
O–C–C	498.2	456.5
O–C–H	468.9	460.8
C–O–C	623.8	467.1

Torsions (kJ/mol)	$u^{torsion}(\phi_{ijkl}) = -0.5\sum_{k=0}^{3} a_k \cos(k\phi_{ijkl})$			
	a_0	a_1	a_2	a_3
O–C–C–H	1.164	0.000	0.000	−1.164
H–C–O–H	1.164	0.000	0.000	−1.164
C–O–C–H	3.382	0.000	0.000	−3.382
O–C–C–O	10.886	0.209	−10.676	0.000
C–O–C–C	8.457	−4.187	−2.931	−1.340

Nonbonded interaction	$u^{nb}(r_{ij}) = A_{ij}\exp(-B_{ij}r_{ij}) - \dfrac{C_{ij}}{r_{ij}^6} + \dfrac{1}{4\pi\varepsilon_0}\dfrac{q_i q_j}{r_{ij}}$			
	A_{ij} (kJ/mol)	B_{ij} (Å)	C_{ij} (kJ/mol Å^6)	q_i(e.c.)
C–C	62 701.5	3.090	2682.9	−0.163,−0.1065[a]
O–O	317 547.0	4.063	1670.0	−0.256
H–H	11 093.3	3.740	114.6	0.097,0.0355[b]
C–H	18 087.0	3.415	578.8	
C–O	141 105.2	3.577	2116.7	
O–H	59 352.0	3.902	437.4	

[a]The second entry is for end group CH_3 methyl carbon atoms.
[b]The second charge is for end group CH_3 methyl hydrogen atoms.

tron spin-echo experiments. As far as we know, no coarse-grained models have yet been proposed for PEO.

In this paper, we adopt the EA force field of Smith and co-workers and the UA force field of van Zon *et al.* and propose a CG model for PEO which is derived using a procedure applied previously.[18] We then perform a series of comparisons on the structure and dynamics of PEO above the melting temperature using the three models. Model performance is evaluated based on agreement with neutron measurements of both structural and dynamic observables.

The outline of this paper is as follows. In Sec. II we give the details of the computational models, while in Sec. III the details of the experiments (neutron diffraction and quasielastic neutron scattering) are discussed. The comparison of PEO structure between different simulation models and neutron diffraction experiments is given in Sec. IV, while in Sec. V comparisons of dynamics are discussed. In Sec. VI a summary and conclusion are given.

II. SIMULATION DETAILS

A. Model

All the simulations were performed on a system of 27 chains with the structure of $CH_3-CH_2-[OCH_2CH_2]_{29}$ $-OCH_2CH_3$ at 343 K. The PEO chains thus consist of 92 backbone atoms and have a molecular weight of 1350 g/mol. The constant-temperature method using the velocity-rescaling algorithm of Berendsen *et al.*[25] was employed. The cut-off distances for the nonbonded interactions are 10 Å in UA simulations, 7 Å in EA simulations, and 13.75 Å in CG simulations.

The force fields for the united atom model are obtained from Refs. 26 and 27, and those for the explicit model are taken from Ref. 28. They are summarized in Tables I and II. In both cases, the Ewald summation method was used to calculate the long-range Coulomb interactions and the mul-

TABLE III. Corresponding time step for different interactions.

Interaction type	Time step (fs)
Bonding, bending, and torsion	1
van der Waals and the real part of the Coulomb Ewald summation	2
Reciprocal part of the Coulomb Ewald summation	4

tiple time step reversible reference system propagator algorithm[29] as detailed in Table III was adopted to speed up the computation.

We discuss preparation of the UA sample first because the UA carbon/oxygen positions are used as the starting coordinates for the EA simulation. The initial configuration of one UA polymer chain is generated by a pivot Monte Carlo sampling procedure.[30,31] Copies of this relaxed chain are placed in a box large enough to prevent chain overlap. The molecular dynamics program is run with the box size gradually decreasing to the desired value set by the polymer density[32] at the desired temperature. To get the initial configuration for the EA simulation, hydrogen atoms are inserted based on equilibrated carbon and oxygen positions from the UA model by fixing the angles between the C–H bond and the backbone C–C or C–O bonds at 110° and the C–H bond length at 1.09 Å. We also use this method to reinsert hydrogen atoms to UA configurations when it is required for comparison to neutron measurements.

To coarse grain PEO, we consider every other oxygen atom as a coarse-grained center, i.e., six united atoms are replaced with a coarse-grained bead. We use distribution functions from the UA simulation to parametrize the coarse-grained force field. Coarse-grained stretching and bending potentials are assigned by Boltzmann inverting distributions obtained from UA simulations. The distribution of CG bond lengths is calculated from the positions of united atoms separated by one CG bond (i.e., 6 united atoms), while that of CG bond angles is calculated from the positions of united atoms separated by two CG bonds (i.e., 12 united atoms). The distribution of torsion angles separated by three CG bonds is featureless; therefore a torsional potential is not used. Figure 1 compares the bond length and angle distributions obtained from the CG simulation with the UA distributions used to assign them. The nonbonded interaction between the beads is parametrized by requiring agreement between the UA and CG intermolecular pair distribution function $g^{inter}(r)$. While in UA simulations, a Lennard-Jones 6-12 potential is used, we find that a 6-8 potential is required in the CG case; otherwise good agreement cannot be achieved. Figure 2 illustrates the comparison of $g^{inter}(r)$ from UA and CG simulations. We present all CG parameters in Table IV. The CG beads are electrically neutral, and thus no Coulomb interactions are used.

B. Equilibration

All systems are equilibrated for at least 2 ns before collecting data, followed by production runs of 4 ns for the EA and UA simulations and 15 ns for the CG simulation. In all the cases, the atoms have moved at least $1R_g$ during the
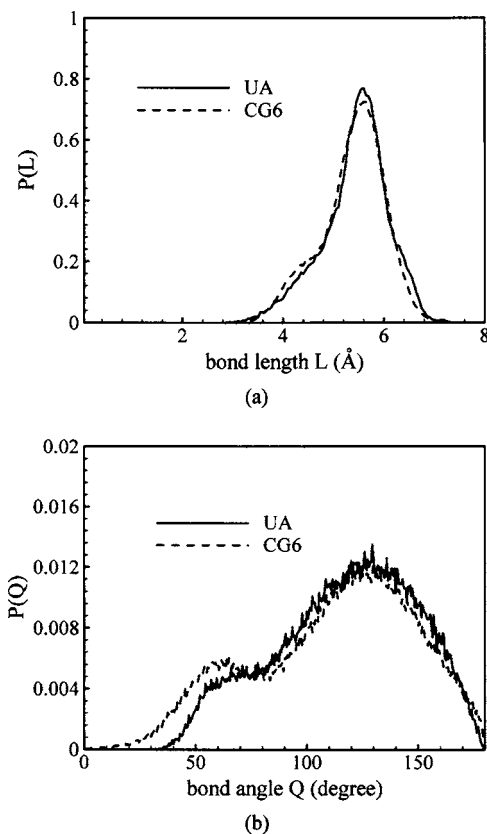

FIG. 1. Comparison of distribution functions from UA and CG simulations: (a) bond length; (b) bond angle.

equilibrium period, and no drifts in structural properties $[g^{inter}(r)]$ are evident. As a further test of equilibration, we choose a dynamic observable, the self-intermediate scattering function $S(q,t)$, and calculate its value over three 1 ns blocks following the proposed equilibration of 2 ns. As shown in Fig. 3, no drifts are observed, suggesting that the equilibration time is sufficient. Similar results are obtained for the other models.

Comparison between the CG simulation and neutron experiments requires reinserting the missing carbon, oxygen, and hydrogen atoms to the CG coordinates. To accomplish this, we use a three-step procedure. First the missing carbon and oxygen atoms are reintroduced using an optimization routine to minimize the sum of bending and dihedral angles
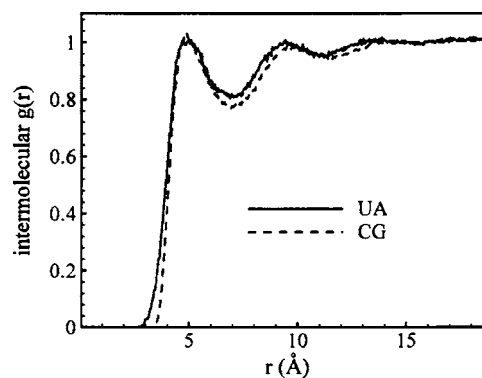

FIG. 2. Comparison of the intermolecular $g^{inter}(r)$ from UA and CG simulations.

TABLE IV. Parameters for CG simulations.

Bonds	$u^{bond}(L_{ij}) = A\exp[-k_1(L_{ij}-L_{01})2] + B\exp[-k_1(L_{ij}-L_{02})^2]$					
	k_1 (Å^{-2})	k_2 (Å^{-2})	L_{01} (Å)	L_{02} (Å)	A (kJ/mol)	B (kJ/mol)
	2.387	3.000	5.603	4.392	3.048	0.599
Bends	$u^{bend}(Q_{ij}) = A\exp[-k_1(Q_{ij}-Q_{01})^2] + B\exp[-k_1(Q_{ij}-Q_{02})^2]$					
	k_1 (rad^{-2})	k_2 (rad^{-2})	Q_{01} (rad)	Q_{02} (rad)	A (kJ/mol)	B (kJ/mol)
	1.875	9.000	2.207	1.116	0.052	0.015
Nonbonded interaction	$u^{nb}(r_{ij}) = 3\varepsilon_{ij}\left[\left(\dfrac{\sigma_{ij}}{r_{ij}}\right)^8 - \left(\dfrac{\sigma_{ij}}{r_{ij}}\right)^6\right]$					
	σ_i (Å)			ε_i (kJ/mol)		
	5.50			0.167		

while keeping the bond distance fixed at 1.54 Å. The system is then relaxed with a short UA simulation (10 ps). This relaxes the positions of the reinserted atoms without significantly altering positions returned from the CG simulation.[10,18] Finally the missing hydrogen atoms are reinserted as described above.

III. EXPERIMENTAL DETAILS

A. Neutron diffraction

Neutron diffraction experiments were performed on perdeuterated PEO ($M_w = 460\,000$ g/mol) at the NIST Center for Neutron Research in Gaithersburg, MD. The sample used was perdeuterated to avoid the large incoherent signal from hydrogen, and ensure that the scattered intensity is dominated by coherent scattering. The BT-7 triple-axis spectrometer was employed with the standard configuration of a double-crystal pyrolytic graphite monochromator and an incident wavelength of 2.47 Å. A 5 cm thick pyrolytic graphite filter was employed to suppress higher order wavelength contaminations. Natural collimation was used before the sample with an effective divergence of 30′ and a Söller slit collimator of 27′ full width at half maximum. The sample was mounted in an aluminum sample holder and in a closed-cycle refrigerator. The investigated q range is from 0.5 to 3.9 Å^{-1}, and the temperature measured is 343 K.

B. The disk chopper spectrometer (DCS)

Time of flight measurements were performed on the disk chopper spectrometer[33] also at the NIST Center for Neutron Research. In this case hydrogenated PEO ($M_w = 463\,000$ g/mol) was used, so that the large incoherent cross section of hydrogen ensures that the signal from the DCS measurement is dominated by self-motion of the hydrogen atoms. The spectrometer was operated at an incident wavelength of 4.2 Å and at a resolution of 0.08 meV (full width at half maximum). The sample is annular in shape and held in a thin-walled aluminum can mounted onto a closed-cycle refrigerator. Sample thicknesses were kept around 0.2 mm to achieve transmissions of $\approx 90\%$ and avoid mul-

tiple scattering effects. The instrumental resolution was measured using a vanadium sample at 295 K and the same instrument configuration. The measured quasielastic neutron scattering (QENS) spectra collected over 6 h periods were corrected for detector efficiencies using software developed at NIST (data analysis and visualization environment, DAVE).[34] Subsequently, the scatterings from the empty aluminum can and from the background were subtracted and the data were binned into q groups in the range of 0.60–2.60 Å^{-1}.
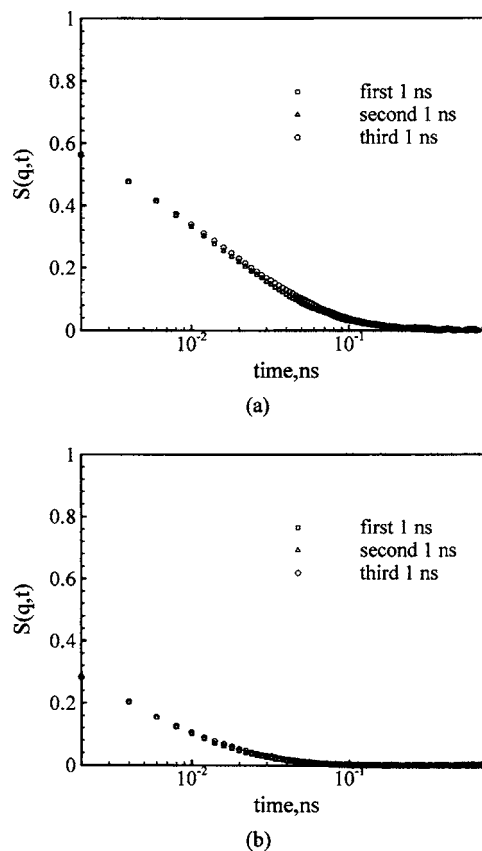

FIG. 3. Self-intermediate scattering function from the EA model of PEO calculated over 1 ns blocks at two q values: (a) 1.5 Å^{-1}; (b) 2.3 Å^{-1}.
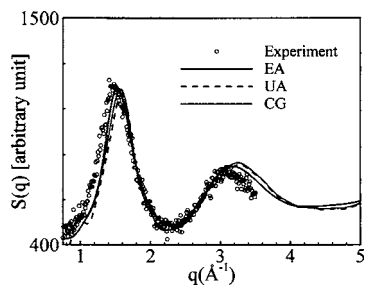
FIG. 4. Comparison of the static structure factors of PEO from UA, EA, and CG simulations and neutron diffraction experiments at 343 K.

IV. LOCAL STRUCTURE AND CHAIN CONFORMATION

In this section we present results on the structure and conformational properties of PEO melts investigated by EA, UA, and CG simulations, and neutron diffraction experiments. Two levels of comparison are made: testing agreement with experiment by reinserting missing atoms and assessing the potential for obtaining information from the coarser models without need for reinsertion of missing atoms by comparing structural properties calculated from only those atoms that serve as centers for CG beads.

A. Agreement with experiment

For the purpose of comparison between simulation models and diffraction data, the missing carbon, oxygen, and deuterium atoms were reintroduced into the UA and CG systems as discussed in Sec. II. This allows us to calculate an atomistic static structure factor $S(q)$ of an isotropic sample by[35]

$$S(q) = \frac{n}{\langle |b|^2 \rangle} \sum_i \sum_j c_i c_j b_i b_j \int_0^\infty [g_{ij}(r) - 1] \frac{\sin qr}{qr} 4\pi r^2 dr,$$

(1)

where

$$\langle |b|^2 \rangle = \sum_i c_i |b_i|^2.$$

(2)

Here i and j represent different atomic species, the coherent scattering length b describes the interaction between neutron and nucleus, the momentum transfer q defines the spatial scale, c is the atomic species concentration, and the radial distribution function $g_{ij}(r)$ reflects the total local packing between atoms of types i and j.

The scattered intensity for PEO as calculated from Eq. (1) and as measured by neutron diffraction is shown in Fig. 4. For the simulation data, we show $S(q)$ calculated from EA, UA, and CG simulations with all the missing atoms reinserted. Because many factors (neutron flux, incoherent background, etc.) influence the scattering intensity from diffraction experiments, the arbitrary rather than absolute coherent intensity is obtained. The incoherent background may be removed with polarization analysis, but BT7 is not equipped to do so. To evaluate agreement between simulation $S(q)$ and neutron diffraction, we match the intensity of the first peak at $q=1.5$ Å^{-1}, and then compare the shapes of the two curves. The spectra obtained from the simulation closely follow the
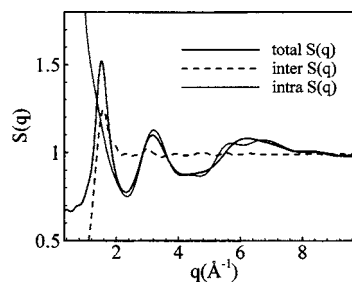

FIG. 5. Inter- and intramolecular contributions to the total structure factor $S(q)$ from EA simulations.

actual diffraction pattern and there is no evidence of crystallinity. This indicates that all the simulation models capture the packing characteristics of PEO melts. Agreement of the value of CG model over distances less than ∼5 Å^{-1} (both the CG bond length and nonbonded σ) indicates that our procedure for reinsertion of the missing atoms is adequate. Figure 4 also shows that pure PEO is characterized by a first peak at $q=1.5$ Å^{-1}, and a second peak at $q=3.0$ Å^{-1}. As expected and presented in Fig. 5, with EA simulation as an example, the origin of the first peak is intermolecular, while the second peak is consistent with intramolecular packing.

B. Comparison between simulation models

Here we compare results from the three models without inserting the missing atoms. As discussed above, the centers of CG beads are located at every other oxygen in the chain. Thus for the EA and UA models, we use only those positions in the following calculations. The intermolecular $g^{inter}(r)$ for all three simulation models are shown in Fig. 6. The UA and CG simulations have a single interchain peak, while this peak is split in the EA model. The split does not produce any observable features in $S(q)$ (Fig. 4). The closely matched results between UA and CG simulations indicate that the CG model is successfully mapped from UA potentials. The origin of the difference from the EA model is unclear.

To assess chain dimensions, we calculate the radius of gyration (R_g) and end-to-end distance (R_e) from the three simulation models. In this case, all available atomic positions in each level of description are included. The radius of gyration is determined using
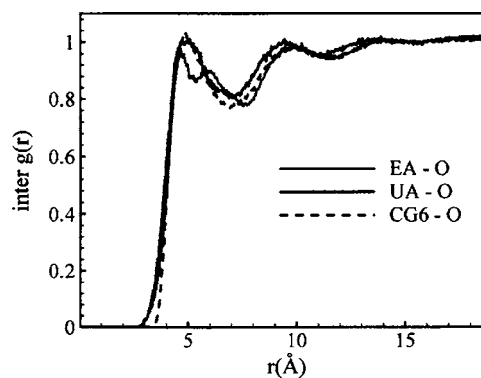

FIG. 6. Comparison of intermolecular radial distribution function $g^{inter}(r)$ for every other oxygen atom from EA, UA, and CG simulations.

TABLE V. Comparison of conformational properties of PEO melts from EA, UA, and CG simulations (errors are standard deviation).

Models (Å)	EA	UA	CG
R_g	10.65±0.53	12.18±0.60	11.00±0.59
R_e	25.80±1.21	30.02±1.58	27.22±1.43

$$R_g = \sqrt{\left\langle \frac{\sum_i m_i (r_i - r_{c.m.})^2}{M} \right\rangle}. \qquad (3)$$

The summation is taken over all the units in a chain (total chain mass M, atom mass m_i), and the average is taken over many coordinate snapshots. The position of unit i is indicated by r_i and the center of mass $r_{c.m.}$ of each chain is $r_{c.m.} = \Sigma_i m_i r_i / M$. Similarly, the end-to-end distance is calculated from

$$R_e = \langle |r_t - r_n| \rangle, \qquad (4)$$

where r_l and r_n are the positions of the first and last carbon atoms on a chain for the UA and EA models, and the first and last CG beads for the CG model. This calculation is also averaged over many coordinate snapshots.

In Table V we compare chain dimensions for the three models. Although in general agreement is good, both R_g and R_e are larger from the UA model than for the CG model. This is reasonable because the first and last united atoms are at the first and last carbon atom positions, while the first and last CG beads are at the first and last oxygen atom positions, making the effective chain length shorter in the CG simulation. Both UA and CG chains are more extended than EA chains. This is also expected, because the equilibrium bond lengths and angles in the EA model for groups involving carbon and oxygen are smaller than their UA counterparts.

V. LOCAL DYNAMICS

A. Mean square displacement (MSD)

The mean squared displacement of individual atoms is evaluated by

$$\Delta r^2(t) = \langle |r_i(t + t_0) - r_i(t_0)|^2 \rangle, \qquad (5)$$

where $r_i(t)$ is the position of atom i at time t and the average is taken over all atoms and multiple time origins t_0. As discussed above, the CG beads are centered on oxygen atoms and thus we compare the mean squared displacement of oxygen atoms in Fig. 7(a).

As observed in Fig. 7(a), the transition from ballistic to subdiffusive behavior is more abrupt in the CG model than in the UA model. As a result, the CG beads have moved further than their UA counterparts for times greater than 0.2 ps. The difference initially grows with time, and then reaches a constant offset. As with our group's work on PE, the time at which offset is reached is identified as the crossover time t_c. The crossover time is material dependent and appears at 15 ps for PE.[18] For PEO t_c is 0.35 ns, as indicated in Fig. 7(a). The importance of t_c is that if we multiply the elapsed time in the CG simulation by a constant value (in this case
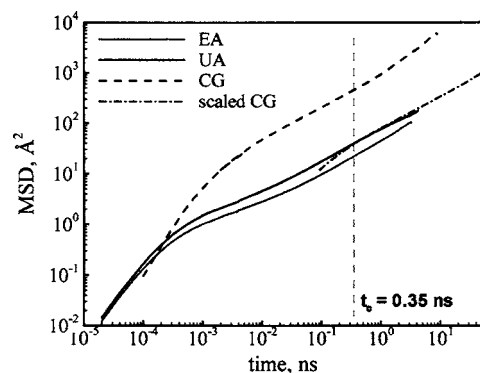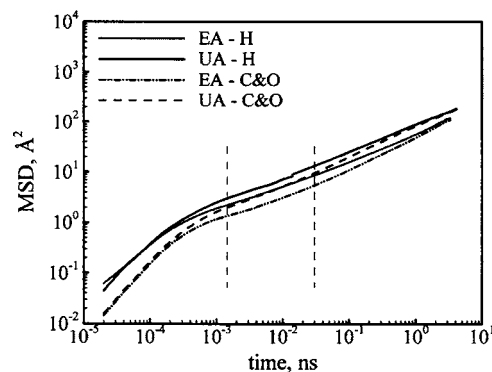
FIG. 7. Comparison of mean square displacements for (a) oxygen atoms from EA, UA, and CG simulations; (b) hydrogen atoms and carbon/oxygen atoms from EA and UA simulations. The region between the two dashed lines indicates the time range for our time of flight measurements.

$\Delta t^* = \alpha \Delta t$ with $\alpha = 53$) the CG curve will overlap the UA curve for $t > t_c$. Presented on a log plot such as in Fig. 7(a), this corresponds to adding a constant to the time axis or shifting the entire curve to the right. As discussed previously,[18] the shifting suggests that in the time range $t > t_c$ any dynamic property computed using scaled time will provide an excellent approximation of the UA simulation. We return to this point below.

Figure 7(a) also shows the mean square displacements of oxygen atoms from EA model. At short times (less than ~0.2 ps), oxygen atoms in the UA and EA simulations move at almost the same speed. The difference grows with time, again reaching a constant offset which is much smaller than that observed between the UA and CG models. We conclude that dynamic properties calculated from the EA model will be slightly faster than those from the UA or CG models.

Since the motion of protons is the relevant variable for comparison to neutron experiments, and they must be reintroduced to the coarser models, in Fig. 7(b) we compare motion of hydrogen atoms in the EA model with motion of the hydrogen atoms that have been reinserted in the UA model. Carbon and oxygen atom motions, which are calculated explicitly in both models, are also shown. The figure illustrates that the difference in mobilities of EA and reintroduced UA hydrogen atoms is similar to that in EA and UA carbon/oxygen atoms, indicating that the reintroduction of protons to the UA coordinates is reasonable. Hydrogen atoms move further than backbone carbon and oxygen atoms. This

is reasonable based on the smaller mass of the hydrogen atoms. At longer times ($\sim$1 ns), the mean squared displacements of hydrogen and backbone atoms move together in both models, as expected because motion at long times represents diffusion of the entire chain. There exists a time range (0.001–0.1 ns) where the UA carbon/oxygen and EA hydrogen atom mean square displacements are coincident. Since this time range represents a major portion of that probed by quasielastic neutron scattering measurements, this suggests that neutron measurements will agree more closely with UA models if the hydrogen atoms are not reinserted. We return to this point below.

B. Incoherent intermediate scattering function

DCS measures the dynamic structure factor $S(q,\omega)$, which is the time Fourier transform of the intermediate dynamic structure factor $S(q,t)$. As discussed above, in hydrogenated PEO, the signal is dominated by incoherent scattering of hydrogen atoms. Although in principle the experiment has a contribution from coherent scattering, this is small ($\sim$3%) and we do not include it. $S(q,t)$ can be determined for all atoms from simulation trajectories. The incoherent intermediate scattering function is calculated directly in reciprocal space:

$$S(q,t) = \frac{1}{N}\left\langle \sum_{i=1}^{N} \exp[-i\mathbf{q}\cdot(\mathbf{r}_i(t+t_0) - r_i(t_0))] \right\rangle$$
$$= \frac{1}{N}\left\langle \sum_{i=1}^{N} \cos(q\cdot|x_i(t+t_0) - x_i(t_0)|) \right\rangle, \quad (6)$$

where $\mathbf{r}_i(t)$ is the distance vector of atom i at time t, and $x_i(t)$ the x coordinate of $\mathbf{r}_i(t)$. For the EA model, this function was calculated using hydrogen atom positions, and again using carbon and oxygen atom positions. The same was done for the UA model after reinsertion of the hydrogen atoms. For the CG simulation, we used the centers of CG beads without reinserting the missing atoms. This is because for all experimentally accessible q values at 343 K, $S(q,t)$ decays to zero before the crossover time of 0.35 ns, after which the CG model is expected to provide accurate dynamics. Thus, after establishing the performance of the UA and EA models by comparison to DCS data, we compare the CG model to the other levels of modeling at two smaller momentum transfers where the decay extends past 0.35 ns.

C. Comparison of simulations with DCS measurement

Plotted in Fig. 8 is the $S(q,t)$ calculated from UA and EA simulation trajectories and measured from DCS experiments at two q values (q=1.5 Å^{-1} and q=2.3 Å^{-1}). As described above, decays calculated using both hydrogen and backbone carbon/oxygen atom positions are shown for each model, for a total of four curves. The most direct comparison is that between hydrogen atom positions in the EA model and DCS experiments. In this case, reasonable agreement is found for times greater than 1 ps. In this time range the UA carbon/oxygen positions also match the experimental data quite well, as anticipated from Fig. 7(b). Surprisingly at
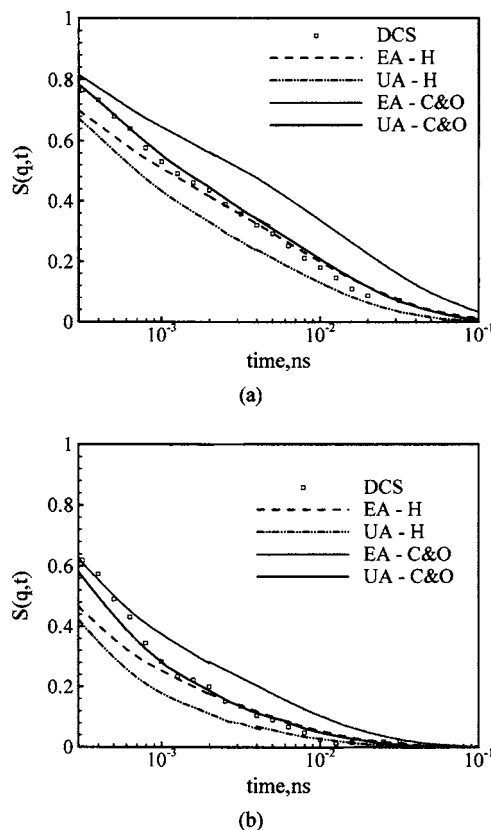

FIG. 8. Comparison of hydrogen atom and carbon/oxygen atom dynamics from EA simulations, UA simulations, and DCS measurements at (a) q =1.5 Å^{-1} and (b) q=2.3 Å^{-1}.

shorter times, the DCS data are in better agreement with the UA carbon/oxygen data than those calculated from hydrogen positions. Although motion from the EA protons most closely represents the QENS data, it appears that the crossover from the ballistic regime occurs too early, and the tail end of this local motion, observable in the DCS data, is missed for EA protons. Since this crossover occurs later for backbone atoms, some of their fast decay appears in this time range such that it best describes the DCS data. As we expect a similar difference in ballistic motion regardless of the system and the coincidence of UA backbone and EA hydrogen motion appears to be related to the exit of the ballistic regime which occurs at nearly the same time for many polymers, we anticipate this correspondence to be observed in many systems where UA modeling is employed. This is indeed the case, as similar observations have been reported in other systems.[36] We conclude that the best description of the experimental data derives from the backbone atoms of the UA model and that the EA hydrogens also provide an excellent description at times greater than 1 ps. The performance of the EA model appears better as q becomes smaller. Clearly, when using a UA model, it is preferable not to reinsert the hydrogen atoms, as the UA-H curve does not provide satisfactory agreement at any time.

While the fast process (times shorter than 1 ps) arises from the unhindered motion in a cage formed by nearest neighbors, the slow process (times longer than 1 ps) originates from the merged α/β process. In order to quantify the
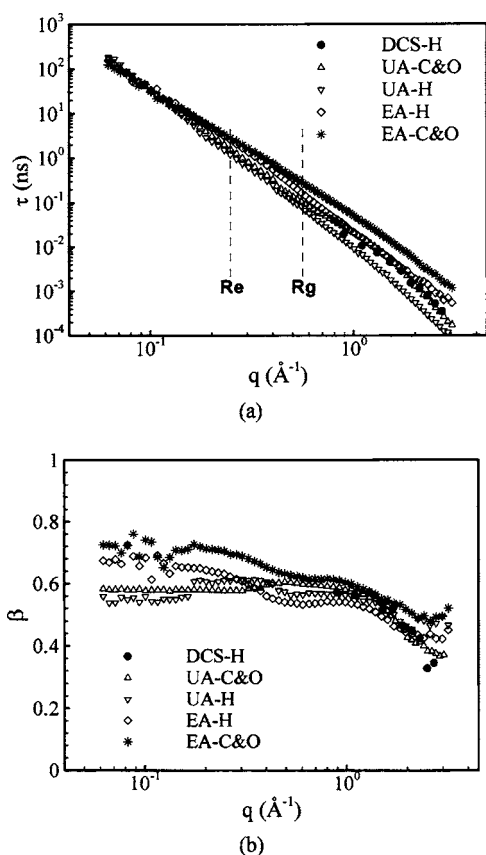
FIG. 9. The q dependence of KWW fitting parameters from EA simulations, UA simulations, and DCS experiments: (a) relaxation time; (b) stretching parameter β.

second process and extend our comparison to all investigated q values, we fit this portion of curve with a Kohlrausch-Williams-Watts (KWW) function,

$$S(q,t) = A \exp\left[-\left(\frac{t}{\tau_{\text{KWW}}}\right)^{\beta}\right], \tag{7}$$

where A is the prefactor, β the width of the distribution, and τ_{KWW} the relaxation time. The resulting fit parameters are reported in Fig. 9 for DCS measurements, and for UA and EA simulations where both hydrogen and backbone motions are considered. We note that at the lower end of the q range depicted in this figure, the small molecular weight of the simulated system likely results in smaller relaxation times than would be obtained from a sample with longer chains. It is clear from Fig. 9(a) that as anticipated above, the relaxation times of UA carbon/oxygen atoms match those from DCS measurements at all available momentum transfers, while the EA hydrogens match for q smaller than 2 Å^{-1}. Relaxation times derived from EA carbon/oxygen atoms and UA hydrogen atoms are not accurate at any spatial scale. At q values greater than the intermolecular packing region ($q < 1$ Å^{-1}), the hydrogen and backbone atom relaxation times for both UA and EA simulations begin to merge, just as their mean squared displacements become coincident at long times. At even larger spatial scales, relaxation times from both levels of modeling merge. Outside the DCS range coincident values of hydrogen and carbon/oxygen relaxation times are apparent for spatial scales comparable to R_e

($q \approx 0.23$ Å^{-1}). This confirms that for whole chain motion, it does not matter which type of atom is tracked. The eventual merging of the two levels of modeling suggests good performance for CG models. Note that the spatial scale corresponding to R_g [indicated by a dashed line in Fig. 9(a)] is not large enough to produce this effect. Within the region where hydrogen and carbon/oxygen times have merged, but UA and EA models are distinct, UA relaxation times are approximately two times faster than those from the EA simulation, indicating a potential disagreement in quantities such as diffusion coefficients.

The scatter in β is larger than that in τ with all values clustered around 0.6. Both EA and UA models seem to adequately capture the experimentally observed distribution of relaxation times. β increases with decreasing q and at larger spatial scales levels off at an almost constant value. The q value at which β begins to level off coincides with that where the backbone and proton relaxation times begin to merge, indicating that reaching a q independence of β is related to whole chain motion. At spatial scales on the order of interchain packing or less, it is more likely for individual atoms to encounter an environment that is locally slower or faster than the average arising from dynamic heterogeneity. As the spatial scale is increased, it will eventually be large enough to include a variety of locally slower or faster environments, which would result in an increasing value for β (smaller distribution), followed by a leveling off when increasing the spatial scale has no further effect. This would suggest that the typical spatial scale of a local dynamic region is less than R_g, and probably comparable to interchain packing.

As discussed above, the CG MSD closely follows that of the UA if the elapsed time for the CG model is taken as $\Delta t^{*} = \alpha \Delta t$ where $\alpha = 53$, provided times larger than the crossover time t_c are considered. Our prior investigation of PE suggests that this observation holds for a range of dynamic properties.[18] Here we use the incoherent intermediate scattering function $S(q,t)$ calculated from oxygen atoms as an example to test this suggestion for PEO. As discussed above, low q values (0.05–0.45 Å^{-1}) are used to compute the scattering function to extend the required decay times past t_c. We first consider $S(q,t)$ calculated at $q = 0.2$ Å^{-1} and $q = 0.3$ Å^{-1} which correspond approximately to R_e and $2R_g$, so they also extend our investigation towards whole chain mobility. Plotted in Fig. 10 is $S(q,t)$ calculated from oxygen positions for all three levels of modeling. Scaled time, $t^{*} = \alpha t$, is used in the plots of CG data. As expected, based on the long time behavior of the MSD, EA oxygen atom dynamics are slower than those for UA. The incoherent intermediate scattering function $S(q,t)$ shows excellent agreement between CG and UA simulations at times longer than t_c. We have fit $S(q,t)$ curves for the slow process using $t > 1$ ps for the UA and EA models and $t > t_c$ for CG model. The results are presented in Fig. 11. Little difference is observed in the β values, and the relaxation times are nearly coincident for the low q range (0.05–0.4 Å^{-1}). Similar results are obtained over the entire q range: CG and UA relaxation times are nearly coincident, while EA relaxation times are greater. The stretching parameters from UA and CG models are similar,
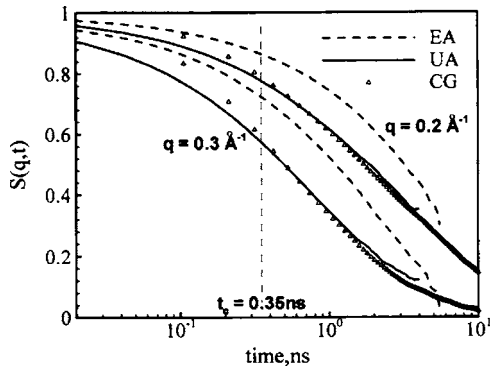
FIG. 10. Comparison of incoherent intermediate scattering function at q = 0.2 Å^{-1} and q = 0.3 Å^{-1} from EA, UA, and CG simulations. Scaled time is used in plotting the CG data.

while that for EA is a little larger at smaller q values (q < 0.5 Å^{-1}). The agreement between UA and CG modeling suggests that once the parameter α is known, CG simulations can accurately predict dynamic properties from UA simulations, and thus can be used to extend the time range possible to evaluate with simulation.

D. Orientation autocorrelation function (OACF)

The orientation autocorrelation function is the frequency Fourier transform of a spectral density function $J(\omega)$ which is measurable in NMR experiments.[39] It describes the decorrelation of the orientation of the C–H bond vector:
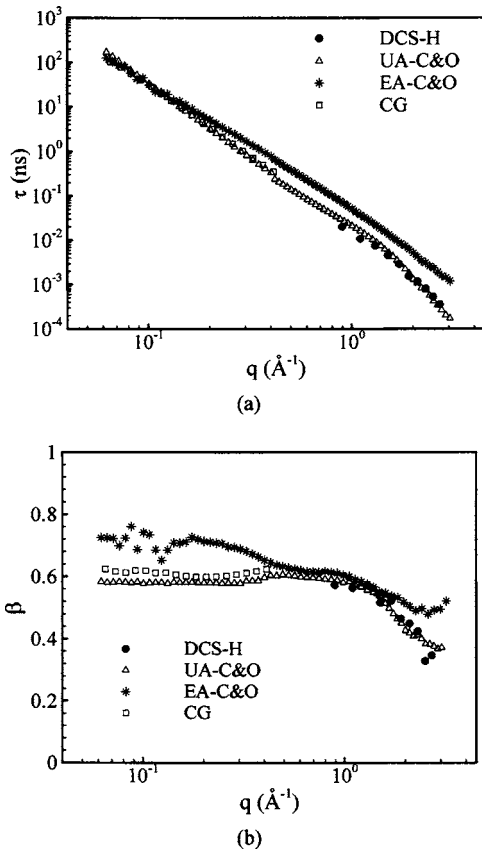

FIG. 11. The q dependence of KWW fitting parameters from EA, UA, and CG simulations and DCS experiments: (a) relaxation time; (b) stretching parameter β.
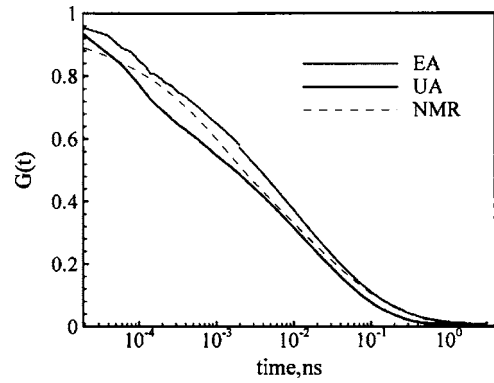

FIG. 12. Orientation autocorrelation functions for C–H vectors calculated at 343 K from EA and UA models and NMR experiments.

$$G(t) = \tfrac{3}{2}\langle \cos^2 \theta(t) \rangle - \tfrac{1}{2}, \qquad (8)$$

where $\theta(t)$ is the angle of the C–H bond at time t relative to its orientation at $t=0$. From the trajectory obtained from simulations, the OACF can be calculated according to Eq. (8). Since the OACF is sensitive to detailed motion of hydrogen atoms and it decays nearly to zero before t_c at 343 K, we do not report results for the CG model. We present $G(t)$ for UA and EA simulations and NMR experiments[39] in Fig. 12. Both the EA and UA models describe the experimental data reasonably well with equal levels of agreement. It is reported that the C–H vector reorientation occurs via two mechanisms, librational and segmental motions, in which case the OACF can be represented by the following functional form,[37,38]

$$G(t) = a_{\text{lib}} \exp\left(-\frac{t}{\tau_{\text{lib}}}\right) + (1 - a_{\text{lib}})\exp\left[-\left(\frac{t}{\tau_{\text{seg}}}\right)^{\beta}\right], \quad (9)$$

where a_{lib} and τ_{lib} are the amplitude and relaxation time for librational motion and τ_{seg} the relaxation time for segmental motion. We fit $G(t)$ presented in Fig. 12 using Eq. (9) with $\tau_{\text{lib}} = 1$ ps as was done in Ref. 39. The resulting parameters are listed in Table VI. The value of a_{lib} is smaller in both the UA and EA representations, indicating the contribution of librational motion is less in the simulation models. Stretching parameters and relaxation times from either simulation model are close to those from NMR experiments. We also report the correlation time for segmental dynamics $\tau_{\text{seg}c}$ which is the time integral of the segmental portion of the correlation function:

$$\tau_{\text{seg},c} = \frac{\tau_{\text{seg}}}{\beta}\Gamma\left(\frac{1}{\beta}\right). \qquad (10)$$

These times, from both simulation models, also closely match the NMR results. We conclude that the local motion

TABLE VI. Comparison of parameters from UA and EA simulations and NMR experiments (Ref. 39).

Models	a_{lib}	β	τ_{seg} (ps)	$\tau_{\text{seg},c}$ (ps)
UA	0.07	0.34	7.9	42
EA	0.05	0.36	11.9	55
NMR	0.10	0.33	10	62

represented in the reorientation of the C–H bond vector can be adequately described by either the EA or UA representation.

VI. SUMMARY AND CONCLUSION

A variety of descriptions is available for chemically detailed simulations of polymer melts. It is desirable to reduce the number of interacting particles in the system so that longer chains may be considered and the simulations extended to longer times. Here we have presented a detailed comparison of three levels of modeling for a polymer, PEO, which is both well studied and has several important applications, including use as a solid polymer electrolyte and as a coating to prevent adsorption of proteins to surfaces. We compare and evaluate the performance of EA, UA, and CG models for both static and dynamic observables, using neutron scattering and NMR data. The EA and UA models are taken from the literature, while the CG model is developed for this comparison. Correct time evolution in the CG model is not enforced by our coarse-graining procedure, instead the elapsed time is scaled by a constant value, which produces coincident mean squared displacements for times greater than a crossover time t_c. We therefore also test agreement between the UA model and the CG model with scaled time for dynamic observables. We find no clear evidence that the EA model provides more accurate results than the UA model for any of the observables considered. The performance of all three models is comparable and in agreement with neutron diffraction for static properties. The dynamics represented via QENS experiments are in reasonable agreement with the EA model. The UA model also performs adequately, but only in the case that backbone carbon and oxygen atom motion is compared to the proton motion probed in the experiment. The dynamics of protons reinserted in the UA simulation do not agree well with QENS data. Both UA and EA data do provide a good description of NMR data, where the performance of both models is comparable. The CG model performs well above the crossover time, which at 0.35 ns, is large enough that the lower levels of modeling are required for comparison to neutron and NMR data. It is reasonable to ask whether the CG model will have continued applicability at longer times, and for larger chain sizes than are explicitly compared with the underlying UA model. We have investigated these issues for PE, and found that a single scaling factor can describe time evolution into the diffusive regime, for chain sizes between 50 and 300 backbone atoms.[40] Diffusion coefficients, tube diameter, and entanglement length are all in reasonable agreement with experimental values. This suggests that the CG model has applicability beyond what is explicitly described above, and thus a combination of approaches where UA modeling is used at short times and CG modeling at longer times will provide an accurate description of dynamic behavior of PEO.

ACKNOWLEDGMENTS

[1] H. Rafii-Tabar and A. Chirazi, Phys. Rep. **365**, 145 (2002).
[2] K. Muralidharan, P. A. Deymier, and J. H. Simmons, Modell. Simul. Mater. Sci. Eng. **11**, 487 (2003).
[3] D. Y. Yoon, G. D. Smith, and T. Matsuda, J. Chem. Phys. **98**, 10037 (1993).
[4] W. Paul, D. Y. Yoon, and G. D. Smith, J. Chem. Phys. **103**, 1702 (1995).
[5] G. D. Smith and D. Y. Yoon, J. Chem. Phys. **100**, 649 (1993).
[6] W. Paul, G. D. Smith, and D. Y. Yoon, Macromolecules **30**, 7772 (1997).
[7] J. D. MCCoy and J. G. Curro, Macromolecules **31**, 9362 (1998).
[8] M. Tsige, J. G. Curro, G. S. Crest, and J. D. McCoy, Macromolecules **36**, 2158 (2003).
[9] W. Tschöp, K. Kremer, J. Batoulis, T. Bürger, and O. Hahn, Acta Polym. **49**, 61 (1998).
[10] W. Tschöp, K. Kremer, J. Batoulis, T. Bürger, and O. Hahn, Acta Polym. **49**, 75 (1998).
[11] K. Kremer and F. Müller-Plathe, MRS Bull. **26**, 205 (2001).
[12] R. L. C. Akkermans and W. J. Briels, J. Chem. Phys. **113**, 6409 (2000).
[13] J. T. Padding and W. J. Briels, J. Chem. Phys. **117**, 925 (2002).
[14] J. T. Padding and W. J. Briels, J. Chem. Phys. **115**, 2846 (2001).
[15] L. Whitehead, C. M. Edge, and J. W. Essex, J. Comput. Chem. **22**, 1622 (2001).
[16] C. F. Lopez, S. O. Nielsen, P. B. Moore, J. C. Shelley, and M. L. Klein, J. Phys.: Condens. Matter **14**, 9431 (2002).
[17] C. F. Lopez, P. B. Moore, J. C. Shelley, M. Y. Shelley, and M. L. Klein, Comput. Phys. Commun. **147**, 1 (2002).
[18] P. K. Depa and J. K. Maranas, J. Chem. Phys. **123**, 094901 (2005).
[19] G. D. Smith, O. Borodin, and D. Bedrov, J. Comput. Chem. **107**, 10446 (2003).
[20] O. Borodin and G. D. Smith, J. Phys. Chem. B **107**, 6801 (2003).
[21] G. D. Smith, R. L. Jaffe, and D. Y. Yoon, J. Phys. Chem. **97**, 12752 (1993).
[22] O. Borodin, G. D. Smith, and R. Douglas, J. Phys. Chem. B **107**, 6824 (2003).
[23] S. Neyertz, D. Brown, and J. O. Thomas, J. Chem. Phys. **101**, 10064 (1994).
[24] A. van Zon, B. Mos, P. Verkerk, and S. W. de Leeuw, Electrochim. Acta **46**, 1717 (2001).
[25] H. J. C. Berendsen, J. P. M. Postma, W. F. Van Gunsteren, A. Di Nola, and J. R. Heak, J. Chem. Phys. **81**, 3684 (1984).
[26] S. Neyertz and D. Brown, J. Chem. Phys. **102**, 9725 (1995).
[27] S. W. de Leeuw, A. Van Zon, and G. J. Bel, Electrochim. Acta **46**, 1419 (2001).
[28] G. D. Smith, O. Borodin, and D. Bedrov, J. Comput. Chem. **23**, 1480 (2002).
[29] M. Tuckerman, B. J. Berne, and G. J. Martyna, J. Chem. Phys. **97**, 1990 (1992).
[30] M. Neal and D. S. Alan, J. Stat. Phys. **50**, 109 (1988).
[31] D. Brown, J. H. R. Clarke, M. Okuda, and T. Yamazaki, J. Chem. Phys. **100**, 1684 (1994).
[32] G. D. Smith, D. Y. Yoon, R. L. Jaffe, R. L. Colby, R. Krishnamoorti, and L. J. Fetters, Macromolecules **29**, 3462 (1996).
[33] J. R. D. Copley and J. C. Cook, Chem. Phys. **292**, 477 (2003).
[34] The IDL-based program can be found at http://www.ncnr.nist.gov/dave
[35] O. Borodin, R. J. Douglas, G. D. Smith, F. Trouw, and S. Petrucci, J. Phys. Chem. B **107**, 6813 (2003).
[36] G. D. Smith, D. Y. Yoon, A. Zirkel, J. Hendricks, D. Richter, and H. Schober, J. Chem. Phys. **107**, 4751 (1997).
[37] B. C. Min, X. H. Qiu, M. D. Ediger, M. Pitsikalis, and N. Hadjichristidis, Macromolecules **34**, 4466 (2001).
[38] X. H. Qiu, N. E. Moe, M. D. Ediger, and L. J. Fetters, J. Chem. Phys. **113**, 2918 (2000).
[39] T. R. Lutz, Y. He, M. D. Ediger, H. Cao, G. Lin, and A. A. Lones, Macromolecules **36**, 1724 (2003).
[40] P. Depa and J. K. Maranas, (unpublished).